Carbon isotopic composition of *Frutexites* in subseafloor ultramafic rocks

Anna Neubeck · Magnus Ivarsson · Curt Broman · Jonathan Lima-Zaloumis ·
Wolfgang Bach · Martin Whitehouse

Abstract Micrometer sized stromatolitic structures called *Frutexites* are features observed in samples from the deep subsurface, and hot-spring environments. These structures are comprised of fine laminations, columnar morphology, and commonly consist of iron oxides, manganese oxides, and/or carbonates. Although a biological origin is commonly invoked, few reports have shown direct evidence of their association with microbial activity. Here, we report for the first time the occurrence of subsurface manganese-dominated *Frutexites* preserved within carbonate veins in ultramafic rocks. To determine the biogenicity of these putative biosignatures, we analyzed their chemical and isotopic composition using Raman spectroscopy and secondary ion mass spectroscopy (SIMS). These structures were found to contain macromolecular carbon signal and have a depleted $^{13}C/^{12}C$ carbon isotopic composition of -35.4 ± 0.50‰ relative to the entombing carbonate matrix. These observations are consistent with a biological origin for the observed *Frutexites* structures.

Responsible Editor: Marguerite A. Xenopoulos.

A. Neubeck (✉)
Department of Geological Sciences, Uppsala University, Uppsala, Sweden
e-mail: anna.neubeck@geo.uu.se

M. Ivarsson
Department of Paleobiology, Swedish Museum of Natural History, Stockholm, Sweden

C. Broman
Department of Geological Sciences, Stockholm University, Stockholm, Sweden

J. Lima-Zaloumis
School of Earth and Space Exploration, Arizona State University, Arizona, USA

W. Bach
MARUM - Center for Marine Environmental Sciences, Universität Bremen, Bremen, Germany

M. Whitehouse
Department of Earth Sciences, Swedish Museum of Natural History, Stockholm, Sweden

Introduction

Frutexites are microstromatolitic structures with a
purported biological origin, and have been reported
from a variety of subsurface environments such as
deep-sea basalts (Bengtson et al. 2014), granitic rocks
(Heim et al. 2017), and marine carbonate caves (Guido
et al. 2016). *Frutexites* display fine-scale lamination
and a directional growth orientation forming columnar
structures and are characteristically composed of iron
oxides and/or manganese oxides and carbonates
(Maslov 1960; Horodyski 1975; Myrow and Coniglio
1991, Heim et al. 2017). As noted by Jakubowicz et al.
(2014) and Guido et al. (2016), *Frutexites* are typically
restricted to environments with low light availability
and low sedimentation, which is consistent within
cryptic deep subsurface environments.

Although *Frutexites* are generally implicated as
products linked to direct or indirect biological pro-
cesses, few reports exist of their immediate connection
to microbial activity. Of these reports, Horodyski
(1975) and Chafetz et al. (1998) reported microfossils
in proximal association with *Frutexites*-like structures
and interpreted their formation as a product of
biologically-induced precipitation. Recent work by
Heim et al. (2017) further explored the microbial
connection and identified active biofilm communities
growing in association with modern *Frutexites*-like
structures, which were shown to contain nitrogen- and
iron oxidizing bacteria as well as Archaea and fungal
biomarkers. Other studies have shown the close
connection between organic matter and trace metals,
where dissolved organic matter in aqueous environ-
ments forms complexes with trace metal ions (Hirose
2007; Rodriguez-Martinez et al. 2011). Organic
matter such as cells and extracellular polymeric
substances have a negatively charged surface that
attract positively charged metal cations (i.e., Mn^{2+}
and Mn^{3+}) to form ligands and complexes (Frankel
and Bazylinski 2003; Sjöberg et al. 2020). Adsorbed
metal cations may eventually become hydrolyzed and
oxidized resulting in the precipitation of metal oxides
(Frankel and Bazylinski 2003), which is a process that

has been implicated in the formation of *Frutexite*-like
structures (Guido et al. 2016).

In this study, we have analyzed *Frutexite*-like
structures composed of Mn-oxides occurring in deep
subsurface ultramafic rock hosted fractures from the
Mid-Atlantic ridge. Identifying fossilized microor-
ganisms and associated structures, such as *Frutexites*,
in the geologic record involves detailed analyses of
micrometer-scale features and the ability to differen-
tiate between biological and abiotic origins of often
cryptic signatures (Benzerara and Menguy 2009).
Multiple lines of evidence are typically required to
determine whether a putative fossil is biogenic,
including identifying characteristic morphological
and chemical signatures, and establishing the overall
habitability of the environment in which the fossil is
found (McLoughlin et al. 2007). To explore the
potential biogenicity of the *Frutexites*-like and micro-
fossil structures reported here, we performed in situ
chemical and isotopic analysis and found evidence
consistent with a biological origin.

Samples and methods

The 1272A 2R1 40–45 cm sample was collected from
the slow-spreading Mid-Atlantic Ridge (MAR) during
Ocean Drilling Program (ODP) Leg 209 at drill hole
site 1272A (Alt et al. 2007; Bach et al. 2004). The The
sample was obtained from a depth of 13.3 m below
seafloor (mbsf) at a seafloor depth of 2560 m below
sea level. The host rocks consist of serpentinized
harzburgite with an approximate age of < 1 Myrs (Alt
et al. 2007; Bach et al. 2004). The sample are
characterized by aragonite veins cutting through the
serpentinized host rock containing putative morpho-
logical biosignatures in the form of microstromatolites
embedded in the aragonite matrix (Ivarsson et al.
2018). Doubly polished thin sections were made from
all samples to identify fossilized microorganisms and
minerals by optical microscopy.

Scanning electron microscopy

Element distribution and imaging were performed
using two different ESEM´s. The first ESEM is a
XL30 Scanning Electron Microscope with a field
emission gun (XL30 ESEM-FEG). The ESEM was
equipped with an Oxford x-act energy dispersive

spectrometer (EDS), backscatter electron detector (BSE) and a secondary electron detector (SE). The second instrument is a Zeiss Supra 35VP (Carl Zeiss SMT, Oberkochen, Germany) field emission SEM, equipped with a VPSE detector for low vacuum conditions, and a Robison BSD for back scatter detection. Also equipped with a EDAX Apex 4 (Ametekh, Mahwah, USA) EDS-detector for X-ray microanalysis. None of the samples were coated.

Raman spectroscopy

Identification of mineral phases and carbon phases were made on the thin sections using a Raman spectrometer using a multichannel Dilor XY spectrometer with an incident laser beam of 514.5 nm and an Innova 70 Ar laser. A Si standard wafer (111) with a Raman peak at 520.4 cm^{-1} were measured daily as a reference prior to the sample analyses. Peak and element analyses were made using INCA Suite 4.11 software. The laser power was determined experimentally but did not exceed 0.5 mW on the organic carbon analyses and the manganese oxides (Fig. 2).

Ion microprobe analyses

In situ carbon isotope analyses were made using the NORDSIM Ion Microprobe (Cameca IMS 1280) at the Department of Geosciences, Swedish Museum of Natural History. The polished samples were mounted on a stainless-steel sample holder and examined with SEM prior to the Microprobe analysis. The SIMS-analysis (10 μm lateral beam dimension, 1–2 μm depth dimension) of carbon isotopes in carbonate and the microstromatolites was performed on a CAMECA IMS1280 ion microprobe. Data were normalized for instrumental mass fractionation using matrix-matched reference materials (S0161, see Supplementary for more details) which were mounted together with the sample mounts and analysed after every sixth sample analysis. Results are reported as per mil (‰) $\delta^{13}C$ based on the PeeDee Belemnite (PDB)-reference value. In total, 18 analyses were made for $\delta^{13}C$ ($^{12}C/^{13}C$) of the sample, divided into two analytical sessions (Fig. 3a and b). The reference material was measured to + 0.22 ± 0.40‰.

Fig. 1 Overview of the thin section sample (**a**) and the overall ▶ composition of the matrix where **b** shows the composition of the aragonite vein, the branched magnetite structures with the included Raman spectra and **c** the EDS spot analyses of the bulk serpentine and aragonite veins

Results

Mineralogy

Sample 1272A 2R1 40–45 cm is composed of serpentine cross-cut by aragonite veins (Alt et al. 2007 and Fig. 1). Spot analyses using SEM showed that the dominating elemental composition was O, Mg, Si and minor Ca and C, whereas the vein composition was dominated by O, Ca and C. Raman spectra of the vein mineralogy is dominated by a major peak at 1085 cm^{-1} and smaller peaks at 155, 207, 706 cm^{-1} corresponding to the reference RRUFF ID R080142 of aragonite (Fig. 1). A few of the matrix analyses showed sharp spectral peaks at 1082 cm^{-1} and minor peaks at 153, 180, 209 and 278 cm^{-1} corresponding to the reference RRUFF ID R050128 of calcite. However, the dominating type of carbonate is aragonite, which has been reported previously (Ivarsson et al. 2018). Black, branching structures in the vein walls was dominated by Raman spectra with only one single peak at 675 cm^{-1}, which can be assigned to the strongest band in magnetite (Fe_2O_4) for green laser (Otero-Lorenzo et al. 2014).

Microstromatolites

At the interface between the host rock and the vein cauliflower-like microscopic structures (Fig. 2a), a few hundred μm in length and up to 50 μm in diameter protrude from the vein walls in a perpendicular fashion and are embedded in the aragonite (Fig. 2a). These structures branch frequently and have an opaque appearance under reflected light microscopy (Fig. 2b). Optical microscopy with a Nikon P-CL 530 nm retardation plate show the structures to consist of dark, magenta colored anisotropic minerals (Nobile et al. 2009) in contrast to the yellowish crystalline aragonite and serpentine (Fig. 2c). EDS analyses (Fig. 2d) and elemental mapping of the sample shows a clear difference between the elemental composition of the microstromatolites (MS) and the rest of the

Elements (wt%)	Spectrum 73	Spectrum 74	Spectrum 75	Spectrum 76	Spectrum 77	Spectrum 78
O	43.8	49.8	51.3	51.1	47.5	47.6
Mg	21.0	21.9	22.8	23.4	5.4	5.0
Si	16.8	16.1	16.8	17.2	2.7	1.7
C	9.8	7.6	5.8	5.4	11.6	12.7
Ca	5.8	3.0	1.7	1.6	30.8	30.8
Fe	2.4	1.3	1.3	1.1	1.2	1.2
Cl	0.2	0.2	0.3	0.1	0.2	0.2
S	0.2	0.1				
Mineralogy	Serpentine	Serpentine	Serpentine	Serpentine	Carbonate	Carbonate
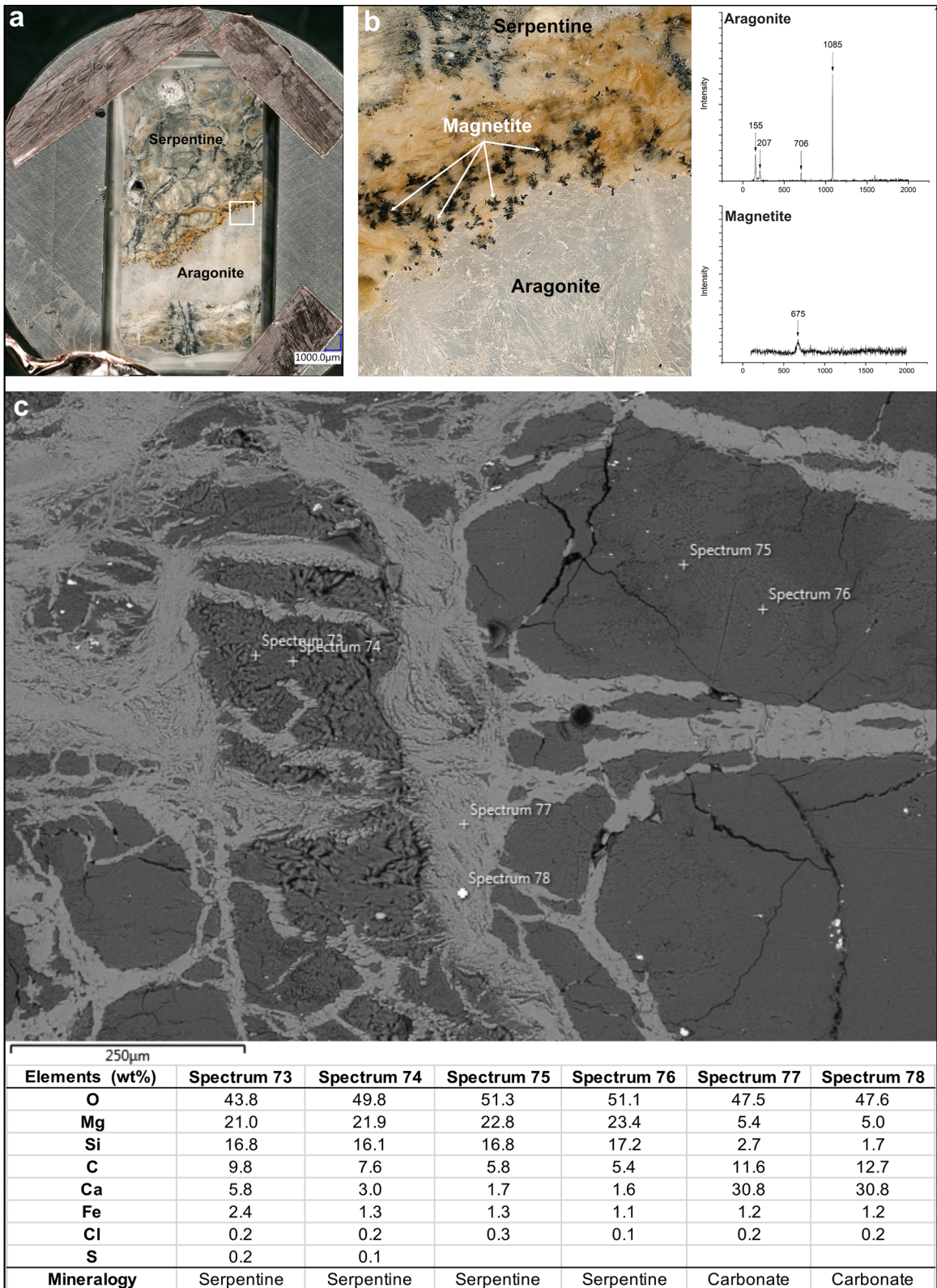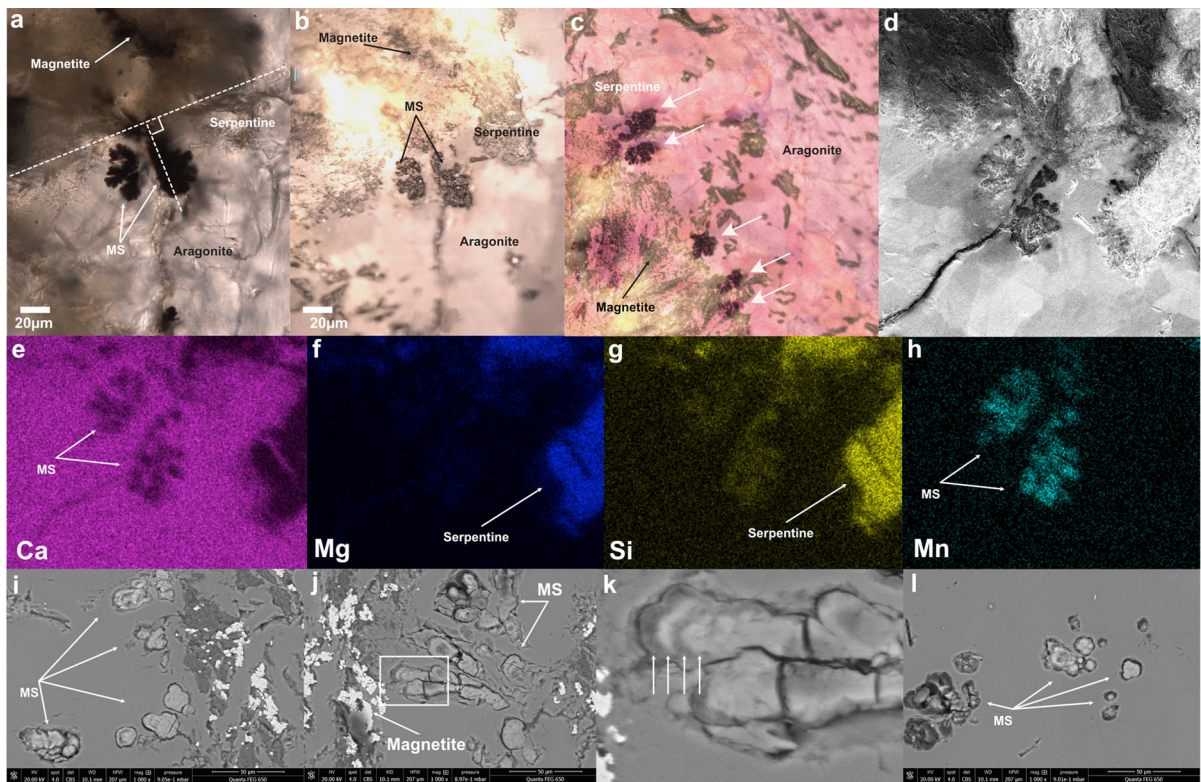
Fig. 2 Overview over the MS´s where **a** shows optical microscopy image of the MS growing perpendicular to the vein walls (marked by dashed lines), **b** shows the MS under reflected light, **c** shows the anisotrophy of the MS using P-CL retardation plate, **d** shows the EDS image of the MS, **e–h** the EDS mapping of the MS and vein walls and **i–l** shows the layered structures of the MS and where the arrows in k marks several of those layers

sample (Fig. 2e–h). The vein walls are composed of Mg, Si, O and Fe whereas the MS is dominated by Mn and O. In cross section, the structures exhibit directional growth and apparent successive layers (Fig. 2i–l).

Raman spectra acquired from the MS (Fig. 3a) showed prominent spectral peaks where the D1 band at $\sim$ 1350 cm^{-1} and the D2 band at 2920–2962 cm^{-1} is visible together with the G-band at $\sim$ 1580 cm^{-1} (Fig. 3b) corresponding to organic carbon (RRUFF ID R120025) and often displaying some degree of fluorescence. Several of the prominent Raman peaks in the MS spectra may be attributed to various Mn phases and species, such as the relatively large and sharp peak at 636 cm^{-1}, which can be ascribed to todorokite (RRUFF ID R0707257, Fig. 3c) and anhydrous manganese oxide [((Na, Ca, K, Ba, Sr)$_{1-x}$(Mn, Mg, Al)$_6$O$_{12}$·3-4H$_2$O)]), Fig. 3d. The MS was dominated by manganese oxides, which was evident EDS analyses (Fig. 3c, d) and in the Raman spectra that

showed peaks at 580 cm^{-1}, which can be assigned to octrahedrally coordinated Mn^{3+} (Bernardini et al. 2021) and/or todorokite (Ostrooumov 2017). A few peaks coincided with sharp spectral peaks at 1082 cm^{-1} and minor peaks at 153, 180, 209 and 278 cm^{-1} corresponding to the reference RRUFF ID R050128 of calcite.

SIMS analyses of putative fossil microstromatolites

In-situ δ^{13}C analyses on the CM using Ion Microprobe *(NORDSIMS)* yielded an average value of − 35.4 $\pm$ 0.50‰ (n = 7, Fig. 4, Supplementary Table 1) compared with the crystalline calcite standard S0161 (Fig. 4), while analyses of the aragonite matrix yielded an average δ^{13}C value of + 0.67 $\pm$ 0.40 ‰ (n = 13, Fig. 4), resulting in a Δ^{13}C of 36.07 $\pm$ 0.64 ‰. Though the absolute δ^{13}C values reported here likely reflect differences in ionization efficiencies

Fig. 3 Raman spectra of the MS where **a** show Bernardini et al. (2021) reflected light image of the MS, **b** shows manganese spectral bands coinciding with carbonaceous matter **b** but is dominated by various types of manganese oxide spectra such as todorokite (**c**) and octrahedrally coordinated Mn^{3+} (**d**)
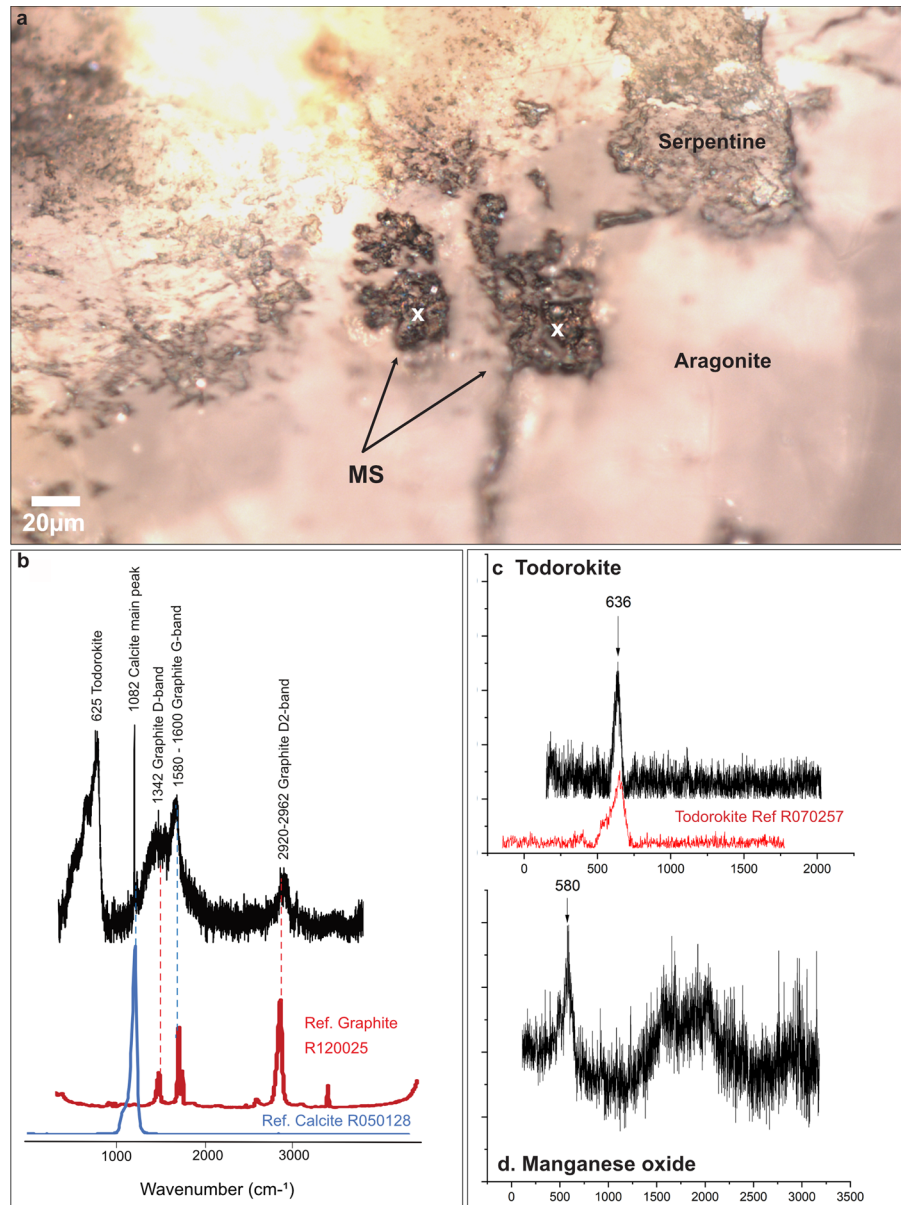
owing to matrix effects, the offset in carbon isotopic composition between the MS structures and the aragonite matrix are clearly significant and correspond to an average offset of $- 36.07 \pm 0.64$ ‰.

Discussion

The fossil record of igneous crust

The deep biosphere (DB) includes organisms living within sediments and igneous rock in both oceanic and terrestrial crust. The DB is estimated to be the second largest reservoir of biomass on Earth representing at least one-tenth to one-third of Earth's total biomass, and is understood to mostly consist of prokaryotic microbial life but also eukaryotes, i.e., fungi
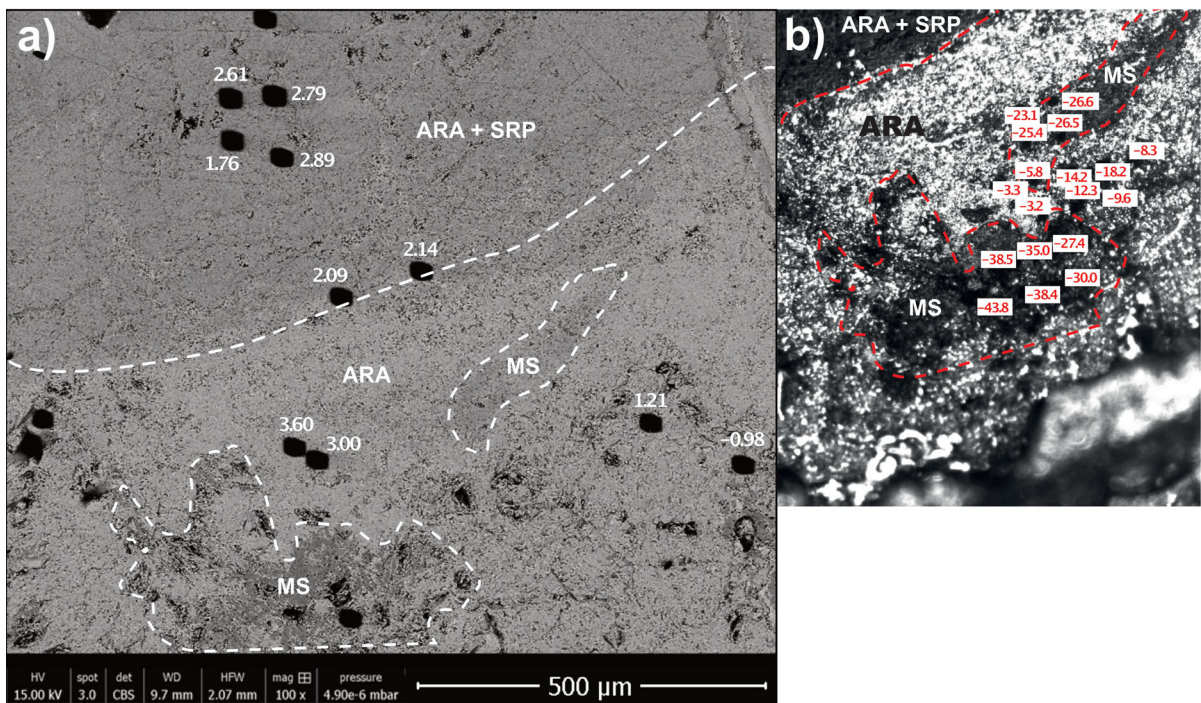
Fig. 4 SEM backscatter image **a** showing the ion microprobe beam spots and the corresponding $\delta^{13}C$ values of the aragonite matrix and **b** the ion microprobe image with corresponding $\delta^{13}C$ ion microprobe measurements of the MS and matrix. The dashed line marks the MS structures. *MS* microstromatolite structure, *ARA* aragonite, *SRP* serpentinite

(Bengtson et al. 2014; Magnabosco et al. 2018). The deep biosphere is still poorly understood, but recent advances in genomic sequencing coupled with the availability of new samples have revealed a surprising diversity of this hidden realm. It is clear that the DB is a substantial reservoir of novel microbial phyla (Magnabosco et al. 2018) and that the interplay between the DB and the surface environments is an important process to all life on Earth. By studying the deep subsurface fossil record, we may further investigate the evolution and distribution of early life on Earth and add to our understanding the interplay between the geosphere and biosphere through time. There is a growing literature of paleo-rock-hosted life from oceanic to terrestrial deep environments and an increased understanding of the biochemical energy flows within this biosphere (Ivarsson et al. 2020).

Microorganisms including fungi are known to colonize rock surfaces, inhabit pore spaces, and utilize the energy released either through direct microbial alteration of rock surfaces or by using the products of abiotic water/rock interactions. Fossilization of these microbes through sudden precipitation of minerals,

such as carbonate or microcrystalline quartz, entombs the microbial colonies in situ. Thus, the fossil rock record not only provides information on the abundance and type of life that inhabits the DB, but also to the extent of their habitable niche environments including fractures, pore spaces and veins within the rock matrix. Raman analyses of the vein filling material surrounding the MS showed that the majority of the minerals was composed of aragonite (Fig. 2). The MS was dominated by manganese oxides, which was evident both in EDS analyses (Fig. 1e–h) and in the Raman spectra (Fig. 3) that showed peaks at 580 cm^{-1}, which can be assigned to octahedrally coordinated Mn^{3+} (Bernardini et al. 2021) and/or todorokite (Ostrooumov 2017), suggesting an oxidizing precipitation environment. Several of the prominent Raman peaks in the MS spectra may be attributed to various Mn phases and species, such as the relatively large and sharp peak at 636 cm^{-1}, which can be ascribed to todorokite and anhydrous manganese oxide. The Mn is present only in the MS and absent in the surrounding rocks (Fig. 2e–h), indicating that the MS have formed through accumulation of Mn

from the fracture fluids. Manganese is common in mafic and ultramafic rocks, constituting approximately 0.16% of the total elemental abundance (Cannon et al. 2017) and have likely been leached to the serpentine fluids during the hydration of the rocks, and subsequently accumulated in the MS. No manganese oxide peaks were found with the Raman analyses other than within the MS. The MS often display broad Raman peaks and sometimes fluorescence, consistent with an amorphous mineralogical composition as well as the presence of organic material and metal oxides (Olcott and Marshall 2015). This anisotropic nature of the MS´s are confirmed by analyses using optical microscopy retardation plate (530 nm, Nobile et al. 2009) showing strong anisotropic colours of the MS, in contrast to the surrounding crystalline aragonite (Fig. 2c). Even though anisotropy is not a biosignature, it is indicative of a different precipitation environment than the closely precipitated branched magnetite or the surrounding crystalline aragonite (Fig. 1). The Raman analyses of the MS showed multiple peaks coinciding with carbonaceous matter (CM), which may have been derived from decomposed biofilms, but that is not possible to discern using 514 nm Raman spectroscopy. The D and G bands are usually used to detect CM of geological samples of various origins, such as microbialites, F*rutexites* and older fossils (Guido et al. 2018, 2019; Allwood et al. 2006; Greco et al. 2018). Close to the vein walls, black mineral structures roughly resembling the MS, were all composed of pure magnetite, likely a product of serpentinization (Fig. 2). Our samples are found in an aragonite vein in an ultramafic oceanic rock that has experienced partial serpentinization (i.e., the hydration of Fe/Mg-bearing minerals and formation of serpentine phyllosilicate phases). Serpentinization is an exothermic reaction capable of releasing a wide range of energy sources for microbial growth, such as H_2, Fe^{2+}/Fe^{3+}, and other metals, and the deep biosphere is to a large extent sustained by the products from serpentinization (Klein et al. 2015; Schrenk et al. 2013).

Biogenicity

To test the biogenicity of the MS, the following criteria was used: geological context and associated habitability, morphology, and chemical (i.e.,

elemental and isotopic) composition. Filamentous fossils have been described in the same sample in a previous study (Ivarsson et al. 2018) where the biogenicity criteria was established for the filaments within the same geological context. The mineral succession with enclosing aragonite indicates that the formation of the MS preceded the precipitation of aragonite and thus grew on the fracture walls while the vein still was open and fluids or seawater circulated the system. This is supported by the lack of alteration rims of the contact between the aragonite and MS. Moreover, the MS do not seem to follow any crystal planes or microcavities, indicating that the MS preceded the aragonite. A dissolution of pre-existing aragonite would have produced an alteration rim surrounding the MS, which was not visible in our samples. As the aragonite formed and sealed the veins, the MS were embedded and preserved in situ. According to Alt et al. (2007), the $\delta^{18}O$ signature of rocks from a nearby drill hole 1272A 2R1 40 are consistent with low-T serpentinization at under 150 °C. Bach et al. (2004) described the presence of the mineral iowaite, which also suggests a low-T regime, forming from Fe-rich brucites during later stages of serpentinization (Bach et al. 2004). Reported formation T < 14 °C (determined using oxygen isotopes) for the aragonite enclosing the MS shows that the T at the time of growth was well within the T range for biological activity (Bach et al. 2004).

The morphology of the microstromatolites is characterized by apparent alternating laminations (Fig. 1i–l), fractal branching growth (Fig. 1), and a distinct direction of growth, which is consistent with previously reported microstromatolites, which have been interpreted as having a biological origin (Guido et al. 2016; Heim et al. 2017). The size distribution of MS reported in these environments are similar to the structures we describe here (Heim et al. 2017; Böhm and Brachert 1993; Myrow and Coniglio 1991). Similar morphologies to the MS´s have been reported by Sjöberg (2019, Fig. 5) in the Ytterby mine in Sweden, where active microbial communities create similar morphologies to the MS and where induced concentration of elements precipitates birnessite-type Mn oxides. Bio-mediated apparent layering, wad like and reticulated morphologies resembling those in our study is also reported in these open mine systems (Fig. 5). Even though abiotic oxidation of Mn^{2+} is possible in such aerobic and slightly basic (pH 8)
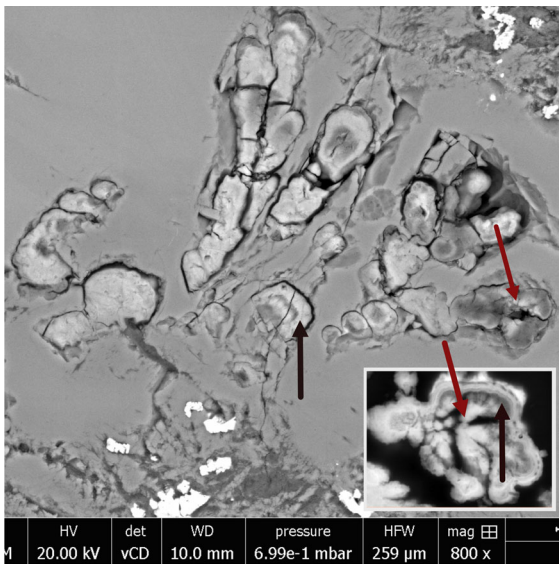
Fig. 5 EDS images showing the morphological similarities between recent, bio-mediated manganese oxides (inset) with its putative laminations (black arrows) and the inner, wad like and reticulated grooves (red arrows). The inset image is modified with permission from Sjöberg 2019 showing manganese oxides mediated by biology in recent natural precipitates on mine walls in Ytterby mine, Sweden. (Color figure online)

environments, it is a considerably slower process than a microbially mediated oxidation of Mn^{2+} to Mn^{3+} (Sjöberg 2019). In mafic/ultramafic systems, fluid pH values are commonly above 8, and at such conditions dissolved Mn^{2+} is partly hydrolyzed, easily adsorbed, and locally concentrated to any available solid surfaces, such as vein walls, cells etc. The trapped Mn^{2+} can then be further oxidized by epilithic or endolithic microorganisms, forming the characteristic morphologies seen in Fig. 5.

These fractally branching bodies are morphologically also very similar to structures that have been previously reported in the literature and identified as *Frutexites*, which are found in cryptic habitats and hydrothermal vents through the Proterozoic and Phanerozoic (Walter and Awramik 1979; Böhm and Brachert 1993) and within subseafloor igneous environments (Bengtson et al. 2014). The nature of microstromatolites has been the subject of continual discussion, with most interpretations in the literature indicating a bacterial origin, however abiotic chemical precipitation has also been considered as an alternative. This question reflects the well-known problem of how to distinguish biogenic stromatolites from non-

biogenic precipitates (Grotzinger and Rothman 1996). Microstromatolitic precipitates in hydrothermal environments are found to range in morphology and structure from bacterially-mediated 'shrubs' to abiotically precipitated dendrites (Chafetz and Guidry 1999). The microstromatolites in sample 1272A 2R1 40–45 are consistent with the first, bacterially formed, category, while microstromatolite structures in the literature ascribed as abiotic are largely dominated by euhedral crystalline forms (Braissant et al. 2003).

Because morphology is merely an indication of biogenicity, additional chemical information of the structures is required to establish a biologic origin. The CM detected by Raman spectroscopy is consistent with biologically derived C in the MS since both the D1 and D2 bands were present (Fig. 3). However, because the presence of D and G Raman bands are only evidence of disordered C and may not represent a definitive biosignature (Allwood et al. 2006), bulk and in-situ $\delta^{13}C$ was also measured. Our in-situ $\delta^{13}C$ measurements of the MS yielded an average value of -35.4 ± 0.50 ‰, while the surrounding aragonite matrix yielded an average value of $\delta^{13}C = 0.67 \pm 0.40$ ‰, consistent with a marine carbonate (Emerson and Hedges 2008). Assuming fractionation proceeded from a common reservoir of dissolved inorganic carbon, the offset between average $\delta^{13}C$ values of CM and aragonite is -36.07 ± 0.90 ‰, which is consistent with fractionation induced by metabolic processes such as the Wood-Ljungdahl pathway or dissimilatory sulphate reduction (Detmers et al. 2001; Londry and Marais 2003). Sulphur isotopes ($\delta^{34}S$) previously measured in the samples had values of approximately -32‰, which were interpreted as resulting from microbial reduction of seawater sulphate via sulphate reducing bacteria (SRB, Alt et al. 2007). Abiotic sulphate reduction was excluded due to kinetic and mass balance mismatches with abiotic processes (Alt et al. 2007). Characteristic fractionation patterns of $\delta^{13}C$ are often cited as strong evidence for biological activity (Schopf, 1993; Ueno et al. 2004), however this interpretation has been challenged by some authors (McCollom and Seewald, 2006). While $\delta^{13}C$ alone may not be strictly sufficient for claiming a biologic origin for microbial structures, a combination of several biologic signatures would provide stronger evidence. SRB have been suggested together with other bacteria such as Fe-reducing bacteria to form microstromatolites as a result of

biofilm mineralization under fluctuating environmental conditions (Krumbein 1983). Based on elemental composition and observed $\delta^{13}C$ and $\delta^{34}S$ isotopic fractionation, we suggest a biological origin of the CM matter within the microstromatolites, and furthermore suggest that signatures are consistent with SRB activity. Energy sources available for microbial colonization and growth are likely derived from serpentinisation reactions where oxidation of reduced Fe species (such as pyroxene and olivine) may reduce water to H_2 through mineral–water interactions. Hydrothermal venting and active serpentinisation is common in the sampled area, with elevated concentrations of both CH_4 and H_2 having been reported (Alt et al. 2007). In combination, the morphological features, presence of carbonaceous material, geologic context favourable for life, in-situ measurements of $\delta^{34}S$ indicative of SRB activity, and in situ $\delta^{13}C$ measured on the MS thus indicates a biologic origin of our microstromatolites (Benzerara and Menguy 2009).

Conclusions

We analysed samples from the Mid-Atlantic-Ridge collected during IODP Leg 209, and found microscopic structures that resembled fossilized *Frutexites*. Observations conducted via microscopic imaging, Raman spectroscopy, and in-situ SIMS carbon isotope analyses indicate a biological origin for these structures. *Frutexites* are typically reported as primarily composed of iron oxides, thus our results broaden our understanding of *Frutexites* to include biogenic structures ofcomposed dominantly of Mn oxides. Additionally, the structures in our samples are found in an ultramafic environment, which is not commonly correlated with *Frutexites*. Combined, our data suggest that the microbial colonization of the deep subsurface is widespread and that similar structures and morphologies can be found in a vast number of different environments.

Data availability All data is presented in the manuscript.

Declarations

References

Allwood AC, Walter MR, Marshall CP (2006) Raman spectroscopy reveals thermal palaeoenvironments of c. 3.5 billion-year-old organic matter. Vib Spectrosc 41:190–197

Alt JC, Shanks WC III, Bach W, Paulick H, Garrido CJ, Beaudoin G (2007) Hydrothermal alteration and microbial sulfate reduction in peridotite and gabbro exposed by detachment faulting at the Mid-Atlantic Ridge, 15°20′N (ODP Leg 209): A sulfur and oxygen isotope study. Geochem Geophys Geosyst. https://doi.org/10.1029/2007GC001617

Bach W, Garrido CJ, Paulick H, Harvey J, Rosner M (2004) Seawater-peridotite interactions: first insights from ODP Leg 209, MAR 15°N. Geochem Geophys Geosyst. https://doi.org/10.1029/2004GC000744

Bengtson S, Ivarsson M, Astolfo A, Belivanova V, Broman C, Marone F, Stampanoni M (2014) Deep-biosphere consortium of fungi and prokaryotes in Eocene subseafloor basalts. Geobiology 12(6):486–496

Benzerara K, Menguy N (2009) Looking for traces of life in minerals. CR Palevol 8:617–662

Bernardini S, Bellatreccia F, Della Ventura G, Sodo A (2021) A reliable method for determining the oxidation state of manganese at the microscale in Mn oxides *via* Raman Spectroscopy. Geostand Geoanal Res 45:223–244. https://doi.org/10.1111/ggr.12361

Braissant O, Cailleau G, Dupraz C, Verrecchia EP (2003) Bacterially induced mineralization of calcium carbonate in terrestrial environments: the role of exopolysaccarides and aminoacids. J Sediment Res 73(3):485–490

Böhm F, Brachert TC (1993) Deep-water stromatolites and Frutexites Maslov from the early and Middle Jurassic of S-Germany and Austria. Facies 28(1):145–168

Cannon WF, Kimball BE, Corathers LA (2017) Manganese, chap. L of Schulz, K.J., DeYoung, J.H., Jr., Seal, R.R., II, and Bradley, D.C., eds., Critical mineral resources of the United States—Economic and environmental geology and prospects for future supply: U.S. Geological Survey Professional Paper 1802, pp. L1–L28

Chafetz HS, Akdim B, Julia R, Reid A (1998) Mn- and Fe-rich black travertine shrubs; bacterially (and nanobacterially) induced precipitates. J Sediment Res 68(3):404–412. https://doi.org/10.2110/jsr.68.404

Chafetz HS, Guidry SA (1999) Bacterial shrubs, crystal shrubs, and ray-crystal shrubs: bacterial vs. abiotic precipitation. Sediment Geol 126:57–74

Detmers J, Brüchert V, Habicht KS, Kuever J (2001) Diversity of sulfur isotope fractionations by sulfate-reducing prokaryotes. Appl Environ Microbiol 67(2):888–894

Emerson S, Hedges J (2008) Carbonate chemistry. In: Emerson S, Hedges J (eds) Chemical oceanography and the marine carbon cycle. Cambridge University Press, Cambridge, pp 101–133

Frankel RB, Bazylinski DA (2003) Biologically induced mineralization by bacteria. Rev Mineral Geochem 54(1):95–114

Greco F, Cavalazzi B, Hofmann A, Hickman-Lewis K (2018) 3.4 Ga biostructures from the Barberton greenstone belt of South Africa: new insights into microbial life. Bollettino Della Soc Paleontol Italiana 57:59–74

Grotzinger JP, Rothman DH (1996) An abiotic model for stromatolite morphogenesis. Nature 383(6599):423–425

Guido A, Rosso A, Sanfilippo R, Russo F, Mastandrea A (2016) Frutexites from microbial/metazoan bioconstructions of recent and Pleistocene marine caves (Sicily, Italy). Palaeogeogr Palaeoclimatol Palaeoecol 453:127–138

Guido A, Russo F, Miriello D, Mastandrea A (2018) Autochthonous micrite to aphanodolomite: the microbialites in the dolomitization processes. Geosciences 8:451

Guido A, Kershaw SA, Russo F, Miriello D, Mastandrea A (2019) Application of Raman Spectroscopy in comparison

between cryptic microbialites of recent marine caves and Triassic patch reefs. Palaios 34:1–11

Heim C, Quéric NV, Ionescu D, Schäfer N, Reitner J (2017) Frutexites-like structures formed by iron oxidizing biofilms in the continental subsurface (Äspö Hard Rock Laboratory, Sweden). PLoS ONE 12:e0177542

Hirose K (2007) Metal–organic matter interaction: ecological roles ofligands in oceanic DOM. Appl Geochem 22:1636–1645

Horodyski RJ (1975) Stromatolites of the Lower Missoula Group (middle Proterozoic), Belt Supergroup, Glaciar National Park, Montana. Precambr Res 2:215–254

Ivarsson M, Bach W, Broman C, Neubeck A, Bengtson S (2018) Fossilized life in subseafloor ultramafic rocks. Geomicrobiol J 35(6):460–467

Ivarsson M, Drake H, Neubeck A, Sallstedt T, Bengtson S, Roberts NMW, Rasmussen B (2020) The fossil record of igneous rock. Earth Sci Rev 210:103342

Jakubowicz M, Belka Z, Berkowski B (2014) Frutexites encrustations on rugose corals (Middle Devonian southern Morocco): complex growth of microbial microstromatolites. Facies 60:631–650. https://doi.org/10.1007/s10347-013-0381-1

Klein F, Grozeva NG, Seewald JS, McCollom TM, Humphris SE, Moskowitz B, Berquó TS, Kahl W-A (2015) Experimental con-straints on fluid-rock interactions during incipient serpentinization of harzburgite. Am Miner 100:991–1002

Krumbein WE (1983) Stromatolites—the challenge of a term in space and time. Dev Precambr Geol 20:493–531

Londry KL, Des Marais DJ (2003) Stable carbon isotope fractionation by sulfate-reducing bacteria. Appl Environ Microbiol 69(5):2942–2949

Magnabosco C, Lin LH, Dong H et al (2018) The biomass and biodiversity of the continental subsurface. Nature Geosci 11:707–717

Maslov VP (1960) Stromatolites. Trudy Inst Geol Nauk Akad Nauk SSR 41:188

McCollom TM, Seewald JS (2006) Carbon isotope composition of organic compounds produced by abiotic synthesis under hydrothermal conditions. Earth Planet Sci Lett 243(1–2):74–84

McLoughlin N, Brasier MD, Wacey D, Green OR, Perry RS (2007) On biogenicity criteria for endolithic microborings on early earth and beyond. Astrobiology 7(1):10–26

Myrow PM, Coniglio M (1991) Origin and diagenesis of cryptobiontic *Frutexites* in the Chapel island Formation (Vendian to Early Cambrian) of Southeast Newfoundland, Canada. Palaios 6:572–585

Nobile C, Carbone L, Fiore A, Congolani R, Manna L, Krahne R (2009) Self-assembly of highly fluorescent semiconductor nanorods into large scale smectic liquid crystal structures by coffee stain evaporation dynamics. J Phys Condens Matter 21:264013

Olcott A, Marshall CP (2015) Vibrational spectroscopy of fossils. Palaeontology 58(2):201–211

Ostrooumov M (2017) Raman and infrared reflection spectroscopic study of mineralogical composition of iron-manganese nodules (Pacific and Indian Oceans). Int J Exp Spectrosc Tech 2:012

Otero-Lorenzo R, Weber MC, Thomas PA, Kreisel J, Salgueiriño V (2014) Interplay of chemical structure and magnetic order coupling at the interface between Cr2O3 and Fe3O4 in hybrid nanocomposites. Phys Chem Chem Phys 16:22337–22342

Rodriguez-Martinez M, Heim C, Queric NV, Reitner J (2011) Frutexites. In: Reitner J, Thiel V (eds) Encyclopedia of geobiology. Springer, Berlin, pp 396–400

Schopf JW (1993) Microfossils of the early Archean apex chert: new evidence of the antiquity of life. Science 80:640–646

Schrenk MO, Brazelton WJ, Lang SQ (2013) Carbon in earth. Rev Mineral Geochem 75(18):575–606

Sjöberg S (2019) Microbially mediated manganese oxides enriched in yttrium and rare earth elements in the Ytterby mine, Sweden, Doctoral dissertation, Stockholm University

Sjöberg S, Stairs CW, Allard B, Homa F, Martin T, Sjöberg V, Ettema TJG, Dupraz C (2020) Microbiomes in a manganese oxide producing ecosystem in the Ytterby mine, Sweden: impact on metal mobility. FEMS Microbiol Ecol 96(11):fiaa169

Ueno Y, Yoshioka H, Maruyama S, Isozaki Y (2004) Carbon isotopes and petrography of kerogens in ~3.5-Ga hydrothermal silica dikes in the North Pole area, Western Australia. Geochim Cosmochim Acta 68(3):573–589

Walter MR, Awramik SM (1979) Frutexites from stromatolites of the Gunflint Iron Formation of Canada, and its biological affinities. Precambr Res 9:23–33